Interfacial Effect Boosts the Performance of All-Polymer Ionic Thermoelectric Supercapacitors

Saeed Mardi, Dan Zhao, Klas Tybrandt, Andrea Reale, and Xavier Crispin*

Ionic thermoelectric supercapacitors (ITESCs) have recently been developed for converting low-grade waste heat into electricity. Until now, most reports of ITESCs have been focused on the development of electrolytes, which then have been combined with a specific electrode material. Here, it is demonstrated that the electrode is not only critical for electrical energy storage but also greatly affects the effective thermopower (S_{eff}) of an ITESC. It is shown that the same ion gel can generate a positive thermopower in an ITESC when using gold nanowire (AuNW) electrodes, while generating a negative thermopower when using poly(3,4-ethylendioxythiophene):polystyrene sulfonate (PEDOT:PSS) electrodes. The achieved negative sign of the S_{eff} could be attributed to the Donnan exclusive effect from the polyanions in the PEDOT:PSS electrodes. After examining the thermovoltage, capacitance and charge retention performance of the two ITESCs, it is concluded that PEDOT:PSS is superior to AuNWs as electrodes. Moreover, a new strategy of constructing an ionic thermopile of multiple p- and n-type legs is achieved by series-connecting these legs with same electrolyte but different electrodes. Using interfacial effect at ionic gels/PEDOT:PSS electrode interface, an enhanced thermoelectric effect in ITESCs is obtained, which constitutes one more step towards efficient, low-cost, flexible, and printable ionic thermoelectric modules for energy harvesting.

1. Introduction

Thermoelectric materials are attractive for converting heat to electricity and vice versa, and have enabled applications in bioelectronics,[1] temperature and humidity sensors,[2] energy harvesters,[3] and refrigeration.[4] Although most thermoelectric materials are based on the diffusion of electrons and holes

S. Mardi, D. Zhao, K. Tybrandt, X. Crispin
Laboratory of Organic Electronics
Department of Science and Technology
Linköping University
Norrköping 601 74, Sweden
E-mail: xavier.crispin@liu.se
S. Mardi, A. Reale
Centre for Hybrid and Organic Solar Energy (CHOSE)
Department of Electronic Engineering
University of Rome Tor Vergata
via del Politecnico 1, Rome 00133, Italy

The ORCID identification number(s) for the author(s) of this article can be found under https://doi.org/10.1002/admi.202201058.

along the temperature gradient, a new class of materials, ionic thermoelectric materials, has recently emerged. In these materials, the thermodiffusion of ions generates a thermovoltage that is orders of magnitude higher than that of classic electronic thermoelectric materials exposed to the same temperature gradient. Electrolytes are today scrutinized as thermoelectric materials due to their low cost, low thermal conductivity, and high thermal and electrical stability.[5] Another major benefit is that the operating temperature is below 250 °C, which includes 50% of all generated waste heat.[6] The ions that thermodiffuse along the thermal gradient are not able to pass into the electronic circuits, and therefore accumulate at the electrode/electrolyte interface, forming an electric double layer. When thermally charging ideal supercapacitors, the stored electrical energy depends quadratically on the thermo-voltage:

$$E = \frac{1}{2}CV_{thermo}^2 \tag{1}$$

where C is the capacitance of the device and V_{thermo} is the generated thermo-voltage which equals to $V_{thermo} = -S_i\Delta T$. Defined as a ratio between the thermo-voltage and temperature difference, a large ionic Seebeck coefficient (S_i) leads to a high amount of stored energy. The charging efficiency of an ionic thermoelectric material operated in an ITESC, without considering the thermal inertia of the material, is related to the ionic thermoelectric figure of merit:

$$ZT = \frac{\sigma_i S_i^2}{\kappa}T \tag{2}$$

in which σ_i is the ionic conductivity, κ is the thermal conductivity, and T is the absolute temperature. In order to improve the performance of ITESCs, numerous approaches have been developed to increase the ionic Seebeck coefficient and ionic conductivity.[7–10] Among the typical ionic thermoelectric materials, polyelectrolytes, ionic liquid-based electrolytes, and their hybrids have attracted significant attention due to their high ionic Seebeck coefficient and decent ionic conductivity.[11]

So far, most researchers have focused on developing novel electrolytes with promising ionic Seebeck coefficient using nonporous metallic electrodes.[9,12] However, due to the small capacitance of the electric double layer at a planar

**ADVANCED
SCIENCE NEWS**

www.advancedsciencenews.com

**ADVANCED
MATERIALS
INTERFACES**

www.advmatinterfaces.de

electrode–electrolyte interface, their applications have been limited to the sensors and thermopiles. In a practical ITESC, the electrode material is critical because a large capacitance can greatly enhance the number of accumulated charges at the electrode/electrolyte interface, i.e., the stored electrical energy. So far, carbon materials such as nanoporous carbon[13] and carbon nanotubes[7] and conducting polymers like polyaniline[14] and PDAQ-BC[15] have been investigated as electrodes in ITESCs. In our recent work, we discovered that the ionic-electronic mixed conductor based on the polymer blends poly(3,4-ethylendioxythiophene):polystyrene sulfonate (PEDOT:PSS) can provide an additional contribution as electrodes in ITESCs.[16] PEDOT is a p-doped π-conjugated polymer that conduct electronic charge carriers, while PSS is an ionic conductor transporting cations. PEDOT:PSS acts as an electrode by connecting the electrolyte to the external circuit through its electronic conduction. On that study, a thermoelectric device composed of two PEDOT:PSS electrodes and an ionic liquid displays a thermoinduced voltage which is affected by the composition of the electrode while keeping the same electrolyte. More especially, the thermoinduced voltage is enhanced with an increasing concentration of PSS in the electrode. This suggested that one origin of the thermo-voltage is interfacial. Since the highly negatively charged PSS selectively facilitates the transport of cation and excludes the entry of anions (Donnan exclusion); we proposed that an extra temperature-dependent potential step at the PEDOT:PSS electrode/electrolyte interface[17] leads to a different voltage drop at the cold and hot sides; thus, resulting in an additional open-circuit voltage contribution when a temperature gradient is applied. The strategy of engineering the electrode/electrolyte interface to maximize the total open-circuit voltage generated by ΔT has yet not been demonstrated for full energy harvesting in ITESCs.

In this work, we demonstrate that the temperature-dependent interfacial effect between PEDOT:PSS and an ion gel can contribute to charge an ITESC together with the ionic Seebeck effect. With AuNW electrodes and the same ionic liquid (IL) electrolyte, the thermo-induced voltage is the opposite of that from PEDOT:PSS electrodes. Hence, p- and n-type ionic thermoelectric legs can be achieved by choosing different electrodes with the same electrolyte. This finding is interesting and emphasizes the essential role of the electrode/electrolyte interface in the overall thermovoltage and thermoelectric charging/discharging. We demonstrate the surprising effect that for the same electrolyte composition, the sign can be changed by the nature of the electrode. Hence, a thermopile of p- and n-type legs electrically connected in series and thermally in parallel can be designed in a new way by considering the nature of the electrodes.

2. Result and Discussion

2.1. Supercapacitor Electrodes and Electrolytes

The electrolytes considered in this study are a series of ion gels containing different amounts of the IL 1-ethyl-3-methyl-1-H-imidazolium bis(trifluoromethansulfonyl)imide (EMIM-TFSI). The ion gel is composed of the copolymer of Poly(vinylidene fluoride-co-hexafluoropropylene) (PVDF-HFP) as a matrix
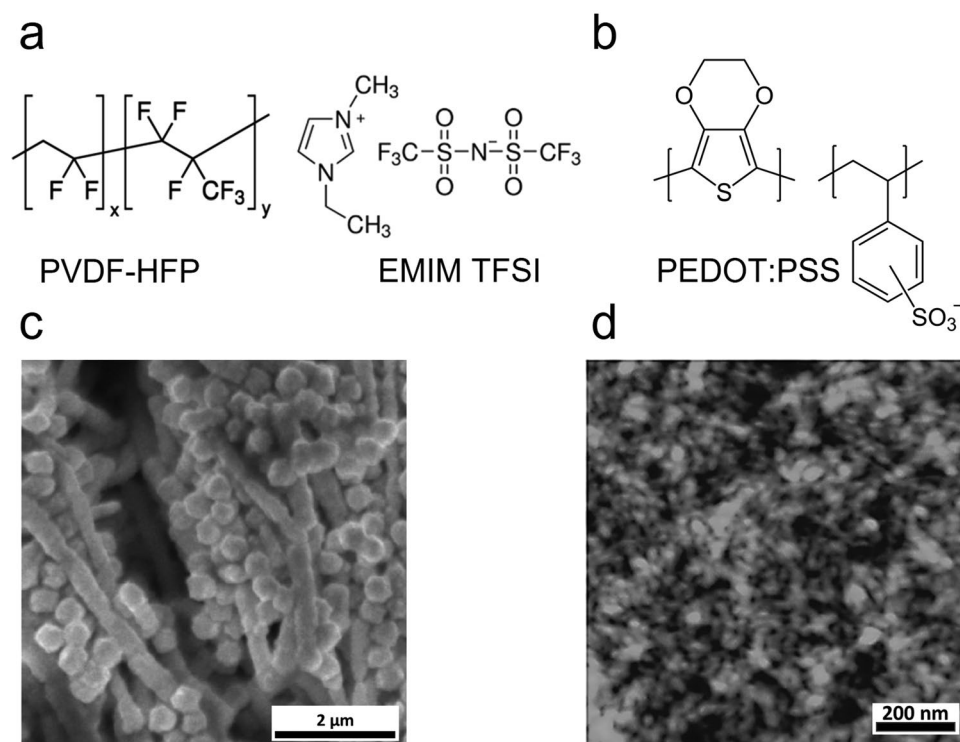

Figure 1. a) The chemical structure of ion gel used in this study. b) The chemical composition of the PEDOT:PSS electrode. Top view morphologies of c) AuNWs (SEM image) and d) PEDOT:PSS (AFM image).
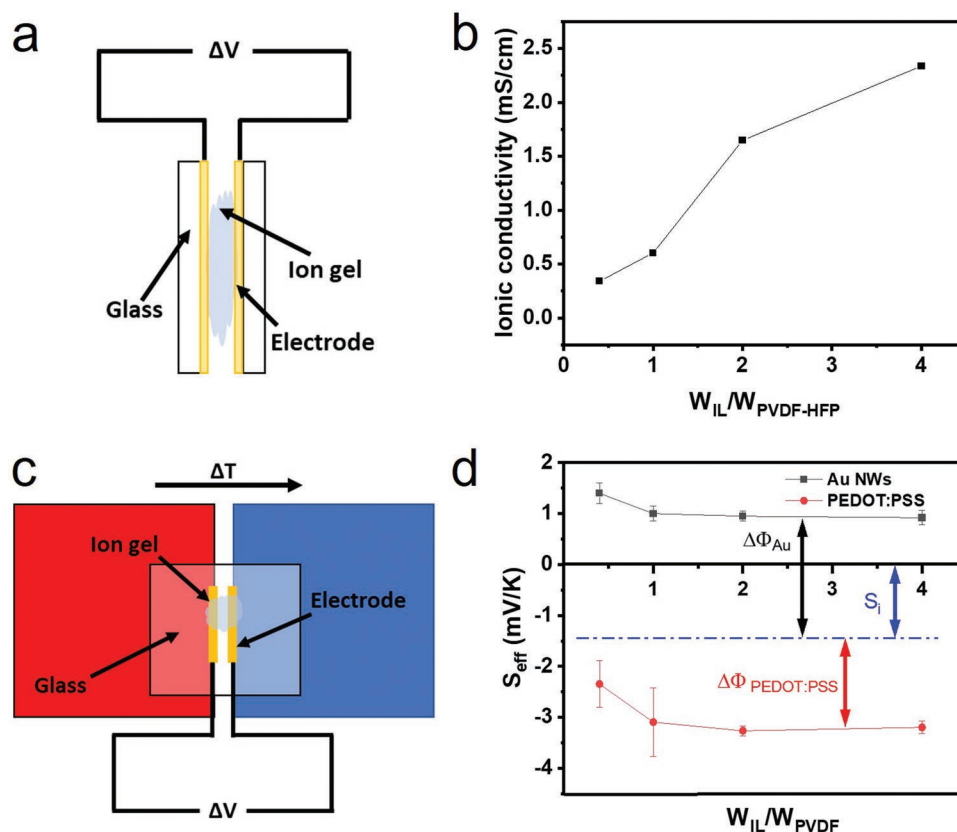
Figure 2. Schematic of the a) vertical and c) lateral structure devices. b) The ionic conductivity of the ion gel electrolytes, measured with PEDOT:PSS electrodes, as a function of $W_{IL}/W_{PVDF-HFP}$. d) The corresponding effective thermopower of the different ion gels and PEDOT:PSS or AuNW electrodes. Inset: S_i, $\Delta\phi_{PEDOT}$ and $\Delta\phi_{Au}$ represent the ionic Seebeck coefficient measured with carbon electrodes, the interfacial potentials of PEDOT:PSS and AuNW electrodes, respectively.

and EMIM-TFSI as the electrolyte (**Figure 1**a). The copolymer includes two phases, the crystalline PVDF segments with the monomer $-(CH_2-CF_2)_x-$ that provide the mechanical strength of the layer; and the amorphous HFP segments with the monomer $-(CF_2-CF(CF_3))_y-$ that can easily absorb the IL. These gel electrolytes have several advantages such as being water-free, nonvolatile, without any liquid leakage, high stability up to 300 °C, and solution processability.[12] We systematically varied the weight ratio of the IL and the polymer matrix: $W_{IL}/W_{PVDF-HFP}$ of 0.4, 1, 2 and 4. As expected, the ionic conductivity of the electrolytes increases with the amount of EMIM-TFSI (**Figure 2**b): 0.34 mS cm^{-1} ($W_{IL}/W_{PVDF-HFP} = 0.4$), 0.60 mS cm^{-1} ($W_{IL}/W_{PVDF-HFP} = 1$), 1.65 mS cm^{-1} ($W_{IL}/W_{PVDF-HFP} = 2$), 2.34 mS cm^{-1} ($W_{IL}/W_{PVDF-HFP} = 4$) (more details on the charge transport of the electrolytes can be found in Note S1 and Figure S1, Supporting Information).

The electrodes considered in this study are layers composed of either PEDOT:PSS or AuNWs. The scanning electron microscopy (SEM) and atomic force microscopy (AFM) images of AuNWs and PEDOT:PSS electrodes are depicted in Figure 1c,d, respectively, clearly displaying that the morphology scale of the conducting domains in AuNWs is about ≈400 nm, while it is about ≈20 nm in PEDOT:PSS. The SEM image of AuNWs shows the compact structure of gold nanowires leading to low sheet resistance (less than 1 Ω/□). The PEDOT:PSS film consists of the conducting PEDOT–PSS cores surrounded

by an insulating PSS shell (Figure 1b). The topography of PEDOT:PSS film illustrates the particles and elongated features on the surface. According to literature, the particles and elongated features represent the conducting parts and insulating domains of PEDOT:PSS, respectively.[18–20]

Simple vertical supercapacitor structures are composed of the ion gel between two electrodes of either PEDOT:PSS or AuNWs (Figure 2a). The ability of those electrodes to store charges is investigated by the cyclic voltammetry (CV) and galvanic charge-discharge (GCD) techniques (Figure S2, Supporting Information). The areal capacitance of PEDOT:PSS electrodes (8.0 mF cm^{-2} at a current density of 24.5 µA cm^{-2}) is higher than AuNW electrodes (0.75 mF cm^{-2} at 14.3 µA cm^{-2}) (Note S2, Supporting Information). Although the two materials are very different, we believe that the difference in capacitance is most likely due to their different morphologies.

Conducting polymers, like PEDOT, are electrochemically active. PEDOT can be oxidized and carrying positive electronic charges (holes) on the π-electron system of the polymer (also called p-doped) that are balanced by negative sulfonate anions of PSS. The oxidized PEDOT:PSS can transport electronic charge carriers and thus conduct electricity. The PEDOT polymer chains form small conducting nanoaggregates that can be considered as a nanoconductor as long as the applied electrochemical potential to PEDOT does not trigger its reduction leading to neutral and non-conducting PEDOT chains.[21] In

**ADVANCED
SCIENCE NEWS**
www.advancedsciencenews.com

**ADVANCED
MATERIALS
INTERFACES**
www.advmatinterfaces.de

the voltage range used in the ITESC device, PEDOT is always highly conducting, such that the charge storage mechanism is based on the formation of electric double layers at the PEDOT aggregate-electrolyte interface,[17] thus a rather similar phenomenon found in supercapacitor with Au nanowires embedded in an electrolyte. Note that both with PEDOT:PSS and AuNWs of lowest *IR* drop, the CV looks like an ideal capacitor with a square box shape $I = -C\,dV/dt$, with C the capacitance and dV/dt the scan rate (Figure S4a, Supporting Information). The galvanostatic charge–discharge is also characterized by nearly triangular shape with small IR drops which also features an ideal capacitive character found with electric double layer formed at electrode–electrolyte interface. Hence, since the AuNW surface has a porous structure with object sizes larger than PEDOT:PSS nanodomains, the electric double layer capacitor built at the interface between the conducting materials and the electrolyte is larger in PEDOT:PSS than in the AuNW electrodes. Note that the capacitance retention of the PEDOT:PSS device is stable (Figure S3, Supporting Information) and the IL content in the electrolytes does not have a significant effect on the capacitance (6.7 mF cm^{-2}, 7.0 mF cm^{-2}, and 7.4 mF cm^{-2} at 16.5 ± 1 μA cm^{-2} for different $W_{IL}/W_{PVDF-HFP}$, respectively of 0.4, 1 and 2) (Figure S4b, Supporting Information). Of course, since the IL concentration has an impact on the ionic conductivity (Figure 2b), it also leads to a variation in ionic resistance in the device and the measured *IR* drop in the GCD curves (13.9, 8.9, 5.0 mV for $W_{IL}/W_{PVDF-HFP}$ respectively of 0.4, 1 and 2, Figure S4b, Supporting Information).

2.2. Contribution to the Thermoinduced Open-Circuit Voltage

We now turn to the measurement of the thermoelectric properties for the lateral device illustrated in Figure 2c. A temperature gradient is applied between the two electrodes and the open-circuit voltage is measured. These devices are labeled as PEDOT:PSS 0.4, PEDOT:PSS 1, PEDOT:PSS 2, PEDOT:PSS 4, AuNWs 0.4, AuNWs 1, AuNWs 2, and AuNWs 4, wherein the numbers refer to $W_{IL}/W_{PVDF-HFP}$. The nearlinear fitting of thermovoltage with temperature difference for both systems indicates that the output thermovoltage is proportional to the temperature difference in the studied temperature range (see Figure S5, Supporting Information). The slope of the fitted linear relationship is the effective thermopower (S_{eff}) which is presented in Figure 2d for the different electrolyte gels. Here, we introduce the "effective thermopower" as a terminology to speak about the voltage divided by the temperature gradient; and this voltage can have other contributions on top of the ionic Seebeck effect based on the thermodiffusion of ions in electrolytes triggered by the Soret effect. When more IL is used in the composition of the ion gel, the effective thermopower of PEDOT:PSS electrodes becomes more negative and saturates at the ratio of 1:1; while for the AuNW electrodes, it becomes less positive and saturates at the same ratio. However, for the ion gels with lower IL content, the low conductivity could limit the ionic thermodiffusion. From the evolution of the potential for PEDOT:PSS electrodes (shown in Figure S6, Supporting Information), we observed that the time needed to establish the thermo-voltage is reduced for

higher IL concentration at the same temperature difference. The sign of the effective thermopower using high IL content is opposite for different electrodes: negative for PEDOT:PSS electrodes ($S_{eff} = -3.3$ mV K^{-1}) and positive for AuNWs ($S_{eff} = +1.0$ mV K^{-1}). These findings imply that the overall thermo-voltage does not only originate from the thermodiffusion of ions in the bulk electrolyte, but also from the additional interaction of ions with the electrodes, which is different in PEDOT:PSS and AuNWs.

For an ionic thermoelectric material, the thermodiffusion of ions along the temperature gradient generates a potential difference (ΔV) between the hot and cold sides (as shown in **Figure 3**a-i,ii,b-i). The thermo-voltage is proportional to the ionic Seebeck coefficient (S_i) and to the corresponding temperature difference (ΔT).[13]

In Figure 3a-ii, the anions thermodiffuse to the cold side more than the cations leading to a lower potential at the cold side compared to the hot side (Figure 3b-i). In such circumstances, the ionic Seebeck coefficient is negative. To probe the ionic Seebeck effect induced thermovoltage, we chose low porosity carbon electrodes because they are not electrochemically active in the potential range used for the ITSECs, and do not promote any chemisorption. For that reason, negligible specific interfacial effects are expected, and the measured thermovoltage should provide the ionic Seebeck coefficient of the bulk electrolyte. For $W_{IL}/W_{PVDF-HFP}$ of 4, the measured Seebeck coefficient of the ion gel is $S_i = -1.4$ mV K^{-1} (Figure S7, Supporting Information). This means that there is an additional interfacial voltage contribution $\Delta\phi_{PEDOT} = -1.9$ mV K^{-1} and an opposite large contribution $\Delta\phi_{Au} = 2.6$ mV K^{-1} for PEDOT:PSS and AuNWs, respectively (Figure 2d).

When one type of ion interacts with the electrodes, an interfacial voltage drop at the electrode/electrolyte interface could have an impact on the resulting thermovoltage:

$$\Delta V = -S\Delta T + \Delta\phi; \text{ where } \Delta\phi = (\phi_H - \phi_C) \tag{3}$$

where ϕ_H (ϕ_C) represents the electrode potential at the hot (cold) temperature. At this stage, more research is needed to truly understand those interfacial contributions, but we can elaborate on some fundamental differences between PEDOT:PSS and AuNW electrodes. As illustrated in Figure 3a-iii,iv, in PEDOT:PSS electrodes that contain PSS polyanions, the Donnan exclusion effect from the negatively charged PSS mainly allows cations to diffuse into the electrodes, thus repelling the anions of the IL accumulated by the ionic Seebeck effect. This results in the potential step at the interface demonstrated previously.[16] It is also possible that the contact of the ion gel with PEDOT:PSS triggers some internal reorganization in PEDOT:PSS and PVDF-HFP to minimize the surface energy, thus resulting in an interfacial dipole. We thus propose a potential profile in the device under the temperature gradient as illustrated in Figure 3b-ii, where both the ionic Seebeck effect and Donnan exclusion interfacial effect would add their contribution to enhance the total thermovoltage.

For AuNW surfaces, we see the opposite interfacial potential drop, illustrated in Figure 3a-v,vi. The difference between anion and cation in adsorption/desorption dynamics on a metal electrode could add an additional term to the thermovoltage.[8] Note
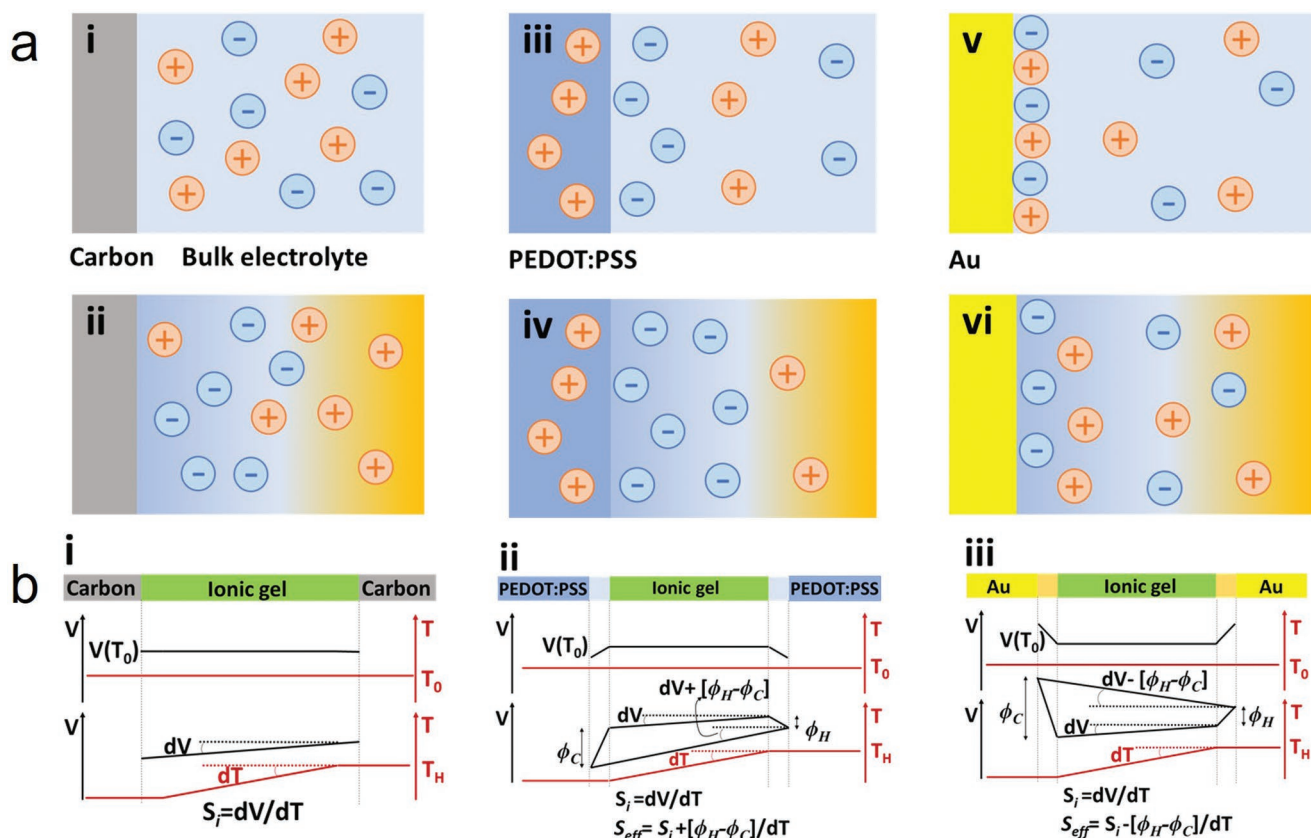
Figure 3. a) The schematic of the ion distributions before and after temperature gradient exposure in the devices with different electrodes: carbon (i,ii), PEDOT:PSS (iii,iv), and AuNWs (v,vi) b) the variation of potential profile with temperature gradient within the electrolyte and at the interfaces of carbon (i), PEDOT:PSS (ii) and AuNWs (iii) electrodes. ϕ_H and ϕ_C represent the magnitude of electrode potentials at hot and cold temperatures, respectively.

that our recent study shows that the water concentration gradient along the temperature gradient could also play a role in determining the ion distribution at the electrode/electrolyte interface.[22] In this work, we indeed found a similar effect for the AuNW electrodes: when decreasing humidity from 35% (room humidity, used for all the measurements unless specified) to 10%RH, the effective thermopower of the AuNW electrodes changes from positive to negative (shown in Figure S8a,b, Supporting Information). On the contrary, the humidity effect is negligible with PEDOT:PSS and carbon electrodes (Figure S8c–f, Supporting Information, respectively). In the PEDOT:PSS and carbon electrodes, reducing the humidity from the measurement chamber leads to the decrease of the thermovoltage. The higher thermovoltage at higher humidity might be due to the diffusion of water molecules into the electrolyte which generates a potential in addition to the thermodiffusion of ions.[23] A recent report mentions that a change in water concentration in LiTFSI can strongly affect the structure of the electric double layer at the Au/electrolyte interface.[24] Thus, regardless of the origin of the interfacial potential on the gold surface, the overall potential profile is shown in Figure 3b-iii. More in-depth investigations are necessary to nail the details of what is happening at the interface and the effect of temperature. However, from our observation, the humidity level mostly affects the ion absorption behavior at the interface between AuNWs and the ion gels, and less with PEDOT:PSS electrodes, possibly because it is highly hydroscopic and could capture water in its bulk.

To further reveal the presence of an interfacial potential contributing to the effective thermopower, we made an asymmetric device of AuNWs-PEDOT:PSS (with similar electrode areas). If there is no difference between the interfacial potential drop at the AuNWs/ionic liquid interface or PEDOT:PSS/ionic liquid interface, we should only measure an extra-voltage of the order of 20–30 μV K^{-1} corresponding to the difference between the Seebeck coefficients of the two electrode materials.[25] But if there is a significant difference in the interfacial dipole at those interfaces, an extra thermovoltage will be measured and should be asymmetric with the direction of the thermal field. This is indeed what is observed in Figure S9 (Supporting Information). Heating up the PEDOT:PSS electrode results in S_{eff} of −3.4 mV K^{-1} (Figure S9c, Supporting Information) while when the temperature gradient is reversed (Figure S9d, Supporting Information), the thermovoltage is −3.0 mV K^{-1}. The 0.5 mV K^{-1} difference originates from the non-identical interfacial drop contribution due to the different nature of the electrodes as presented in the model of Figure 3.

2.3. Thermoelectric Charging of the ITESCs

Because of the superior capacitance, low self-discharge behavior, and weak humidity effect of PEDOT:PSS electrodes compared to AuNW electrodes, we focus on the PEDOT:PSS
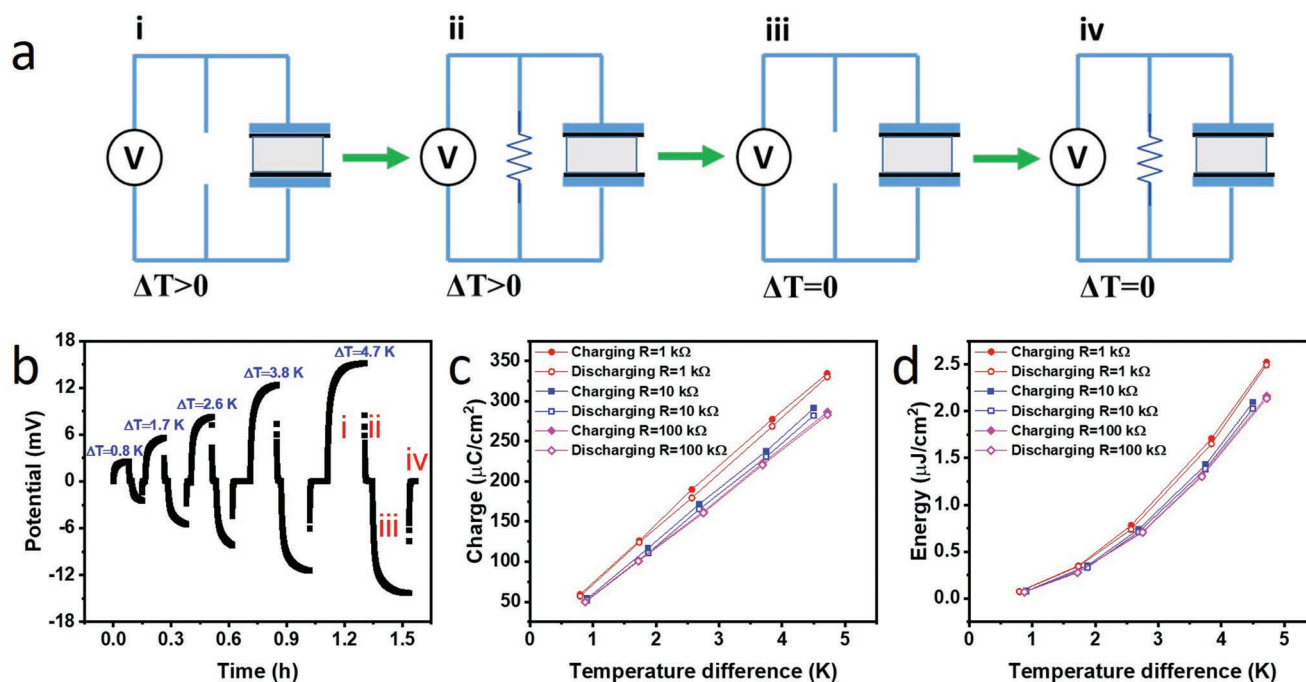
Figure 4. a) The schematic procedure of thermally charging and discharging, i) applying a temperature difference across the device to induce a thermovoltage, ii) the loading of an external resistance and the charging of the device, iii) cooling and removal of the external resistance to reach equilibration, and iv) discharging by loading the resistance. Thermally charging-discharging behavior of b) ITESC-PEDOT:PSS with different ΔT and $R_{load} = 1$ kΩ. The c) charge and d) electrical energy stored in the capacitor during charging and discharging for different values of R_{load} and ΔT.

electrodes and demonstrate an all-polymer ITESC with thermal charging and discharging. As shown in **Figure 4**a, the working principle consists of a series of operation steps: First, a temperature difference is applied between the electrodes to induce a thermovoltage. Second, an external resistance (R_{load}) is connected, which allows the electrons to flow from one electrode to the other driven by the thermovoltage. Hence, the supercapacitor is charged. In the third step, the temperature difference goes to zero to remove the internal thermoelectric potential generated in the electrolyte. As the device is kept in open circuit, the accumulated charges at the electrodes upon charging are maintained and govern the electric potential difference across the device. In this step, if there is no leakage or self-discharge, the obtained potential should be equal but opposite in sign to the initially thermal induced open-circuit voltage. In the last step, the external resistance is loaded again to discharge the device. Figure 4b shows the thermal charging behaviors of ITESC-PEDOT:PSS with different ΔT and the load resistance of 1 kΩ (the graphs with other load resistances, $R = 10$ and 100 kΩ, can be found in Figure S10a,b, Supporting Information, respectively). The identical shape of the thermovoltage in step i) and the open-circuit voltage of the charged ITESC in step iii) confirms the absence of self-discharge phenomenon and thus the good charge storage ability of the all-polymer ITESC. Figure S11 (Supporting Information) displays that the charged open-circuit voltage is maintained for more than 50 hours without significant decay. For the sake of comparison, it is also possible to compare the electrical charging with the thermoelectric charging, the rather similar discharge curves obtained for both charging methods is another evidence of the good ITESC

operation (Figure S12 and Note S3, Supporting Information). The similarity of the discharging behaviors proves that thermoelectric charging is equivalent to an external power supply of the same potential.

By integrating the charging and discharging currents from Equations S1 and S2 in Note S4 (Supporting Information), we can calculate the amount of transferred charge of ITESC-PEDOT:PSS. Figure 4c displays the transferred charges during the charging and discharging processes for different values of R_{load} with increasing ΔT. The fact that both the charge obtained during charging ($Q_{charging}$) and the charge released upon discharging ($Q_{discharging}$) are close to each other indicates that the device has good charge retention. The charge per area increases linearly with the applied temperature gradient according to:

$$Q_{charging} = CV_{charging} = CS_{eff}\Delta T \qquad (4)$$

The Faraday efficiency of the ITESC-PEDOT:PSS is between 96% and 99% for all the resistances and temperature gradients. Note that we made an ITESC device based on the AuNW electrodes, but due to the self-discharge phenomena, its performance was not good. As shown in Figure S10c (Supporting Information), for gold electrodes at $\Delta T = 10.1$ K, $Q_{charging}$ per unit is 26.1 μC cm^{-2} while the discharge releases less than half ($Q_{discharging}/A = 12.01$ μC cm^{-2}); resulting in a Faraday efficiency of only 47%. The self-discharge phenomena for EDLCs could come from three main processes: charge redistribution, faradaic reactions at surface that induce charge transfer reactions at the electrodes, and ohmic leakage.[26] Considering the similarity of the electrolyte, and the fact that carbon and gold
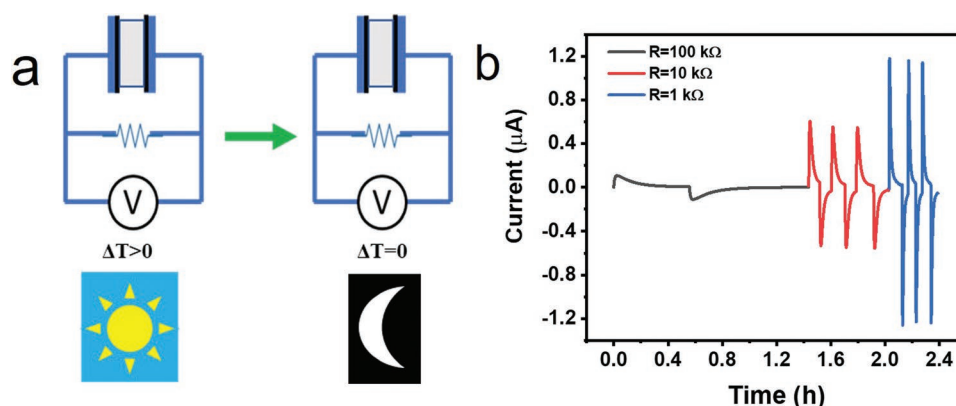
**ADVANCED
SCIENCE NEWS**

www.advancedsciencenews.com

**ADVANCED
MATERIALS
INTERFACES**

www.advmatinterfaces.de

Figure 5. a) The schematic of ITESC device with a loading resistance for continuous power generation, b) the generated currents of ITESC-PEDOT:PSS corresponding to different load resistances. When the device is subjected to a temperature difference, it produces current and the electrical energy can be delivered from that. After the removal of the temperature gradient, the electrical current flows in the inverse direction.

electrode are not forming dendrites, the ohmic leakage current could not be the origin of the extra self-discharge with gold electrodes. As a proposed mechanism, the faradaic reactions might occur due to the reduction of the dissolved oxygen in the ionic liquid at the negatively biased Au NWs electrode.[27,28] In contrast, PEDOT:PSS does not provide electrocatalysis for the fully reduction of oxygen into water.[29] Moreover, the negatively charged PSS shell in PEDOT:PSS might function as an insulator layer that block the electron transfer at the interface and reduce the rate of faradic reaction.[30] These results again show the superiority of PEDOT:PSS electrodes compared to AuNWs.

The stored and released energy during charging and discharging are calculated from Equations S3 and S4 in Note S4 (Supporting Information), respectively. Figure 4d displays the stored electrical energy per area with PEDOT:PSS electrodes, it increases quadratically with ΔT as expected from Equation (1). Considering the capacitance and effective thermopower, we could conclude that the interfacial potential in addition to the ionic Seebeck potential can be used to charge the device (more details can be found in Note S4, Supporting Information). The stored energy during charging with PEDOT:PSS electrodes is extrapolated to be about 11.2 µJ cm^{-2} for $\Delta T = 10.1$ K while it is only 0.157 µJ cm^{-2} for AuNW electrodes at the same temperature gradient (calculated from Figure S10c, Supporting Information). The stored energy in PEDOT:PSS electrodes indicate that these materials could harvest and store energy efficiently when compared with similar systems such as PEO-NaOH/CNT (1.35 µJ cm^{-2} for $\Delta T = 4.5$ K),[7] Pt/EMIM-TFSI (5 nJ cm^{-2} for $\Delta T = 20$ K),[13] ion exchange membrane on activated carbon (AC)/NaCl H$_2$O (0.2 µJ cm^{-2} for $\Delta T = 30$ K),[31] and HEC-EMIM ES/AC (1.75 µJ cm^{-2} for $\Delta T = 11.5$ K).[32]

Because of the zero ΔT requirement in steps (iii) and (iv) in the operation principle, to be able to distinguish charging and discharging unambiguously (see Figure 4a), the ITESC is especially suitable for energy harvesting from intermittent heat sources, but there is no need for its function to be stopped at each of the four steps. **Figure 5**a is a functional mode of operation of this device: different from the four steps of the thermal charging–discharging process which we used to analyze the device performances; the external resistance is here connected to the thermoelectric device constantly. Figure 5b

shows the generated currents in the ITESC-PEDOT:PSS with three different load resistances (100 kΩ, 10 kΩ, and 1 kΩ) at $\Delta T = 5.5$ K. The corresponding potential evaluation is also shown in Figure S13 (Supporting Information). The increase of the resistance diminishes the rate of the charging and discharging process and there should be an optimum for power generation. The possible application of this structure is to continuously charge a larger battery or supercapacitor when there is an intermittent temperature gradient. For instance, during daylight where there is a temperature difference, the device produces the current whereas, during the night where there is no temperature difference the device produces a similar current in the opposite direction. Another possible application could be for the powering of wearable devices where temperature fluctuations occur either by removing the wearable ITESC from the body contact (hot side) or tracking the outside temperature variation (going in and out in wintertime).

2.4. Thermoelectric Complementarity Induced by the Electrode/Electrolyte Interface

In this part, we take advantage of the opposite sign of effective thermopower generated from PEDOT:PSS and AuNW electrodes to demonstrate a simple thermopile. The uniqueness in this thermopile is that the p- and n-type legs are composed of the same thermoelectric ion gel, but it is the nature of the electrodes that drives the change in the thermo-voltage. This underlines the importance of interfacial effect in ITESC which can thus be a new strategy to consider for performance optimization. As shown in **Figure 6**a, the p-leg is made of the AuNW electrodes; while the n-leg is made of the PEDOT:PSS electrodes; both are connected thermally in parallel and electrically in series with silver paste. Unlike most p–n thermoelectric generators, which require thermoelectric materials to have opposite Seebeck coefficients, here, we take the advantage of the thermovoltage determined by different interfacial effects and keep the same ionic thermoelectric material. As shown in Figure 6b, the potentials of the p- and n- legs follow the temperature difference (Figure 6c), but with different signs. The potential of the two connected legs is the sum of the two individual legs. From
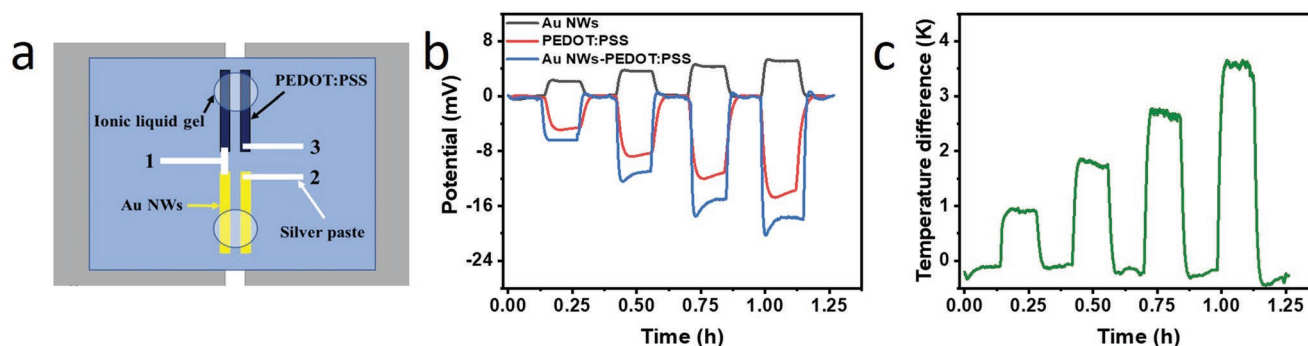
Figure 6. a) The schematic of measurement set up and the series connection of p and n-type elements. Time-dependent variation of b) thermovoltage and c) temperature difference corresponding to PEDOT:PSS, AuNWs electrodes and their series connection. For these measurements, the $W_{IL}/W_{PVDF-HFP}$ is 4.

the linear fitting in Figure S14 (Supporting Information), the effective thermopower of the n-leg, p-leg, and combined legs are 1.10, 3.35, and 4.36 mV K^{-1}, respectively. The comparison of voltages between different electrodes confirms that the series connection of two elements creates a p–n ionic thermocouple. The same strategy can be used to design ionic thermopiles as ultra-sensitive temperature or heat flux sensors.[12]

3. Conclusion

In summary, the performance of ITESCs composed of PEDOT:PSS and AuNW electrodes and nonaqueous polymer electrolyte gel have been investigated and compared. We found out, the electrode/electrolyte interfacial effect has an important role not only for the energy storage, but also for the sign and magnitude of the thermovoltage. Our results confirm that the sign of the effective thermopower can be tuned by using different electrode materials, which is an important supplement for developing p- and n-type thermoelectric legs. The effective thermopower, capacitance, and charge retention for PEDOT:PSS device is superior compared to AuNW device using the same electrolyte. We believe that this study will provide guidance for the future development of ITESCs and efficient ionic thermoelectric modules. Given the simplicity of our approach, a similar strategy seems appropriate to fabricate flexible and large area modules.

4. Experimental Section

Materials: Poly(vinylidene fluoride-co-hexafluoropropylene) (PVDF-HFP, Mn = 130 000) (Sigma-Aldrich), 1-ethyl-3-methylimidazolium bis(trifluoro-methylsulfonyl)imide ([EMIM] [TFSI]) (Sigma-Aldrich), PEDOT:PSS aqueous solution (Clevios PH1000 from Heraeus Holding GmbH), (3-Glycidyloxypropyl)Trimethoxysilane (GOPS) (Sigma-Aldrich), descriptiondimethyl sulfoxide (DMSO) (Sigma-Aldrich), aqueous-based colloidal graphite dispersion (Bonderite L-FG ADAG, Ladd Research Industries), gold(III) chloride solution (Sigma-Aldrich), hydroxylamine (Sigma-Aldrich), titanium dioxide NWs (Novarials, Novawire-TiO-100-RD), poly(dimethylsiloxane) (PDMS) (Sylgard 184, Dow Corning).

The Fabrication and Characterization of Electrodes: The commercial aqueous dispersion of PEDOT:PSS including 0.1wt% of silane crosslinker GOPS and dimethyl sulfoxide were mixed. The ratio of DMSO and

PEDOT:PSS/GOPS was 0.1 and 3%v/v, respectively. The solutions were stirred for a few hours at room temperature. For the fabrication of planar devices, the substrates were patterned by Kapton tape. The PEDOT:PSS electrodes were prepared by drop-casting the solutions on patterned glass substrates. Finally, the films were annealed at 140 °C for 30 min on a hot plate. The preparation process and transferring of AuNWs onto glass have been already reported.[33] Briefly, Gold chloride solution was reduced by hydroxylamine onto titanium dioxide NWs which formed gold coated TiO$_2$-NWs (AuNW, diameter ≈400 nm). AuNW suspension was filtered through a filter membrane, resulting in an AuNW film on top of the membrane. The patterned AuNWs were transferred onto PDMS on glass. After preparing the electrodes, ion gel was drop-casted on them.

The morphology of AuNWs was investigated with a scanning electron microscope (SEM, ZEISS Sigma 500 Gemini). The morphology of PEDOT:PSS was characterized by an atomic force microscope (AFM Dimension 3100) with a silicon probe (resonance frequency of 280 kHz).

The Preparation of the Ion Gel: The ion gels were prepared by mixing IL and acetone solution of co-polymer (PVDF-HFP, $W_{PVDF-HFP}/W_{acetone}$ = 1:7) with different weight ratios. Then it was stirred for 30 min at room temperature. For making the samples, the solution was drop-casted on the electrodes, and dried at 60 °C on a hot plate for 15 min.

Thermoelectric Measurement: The potential difference between the two electrodes was measured with a nano voltmeter (Keithley Instruments, Inc., model 1282 A), connected to the cooling and heating Peltier elements to generate a temperature difference across the edges of the electrodes. The temperature difference was detected and measured using two thermocouples and Keithley 2400 multimeter, respectively. Thermoelectric measurements throughout this study were performed under ambient humidity of ≈40% unless otherwise stated. To study the effect of humidity on the thermo-voltage, the humidity was reduced to less than 10% by purging the nitrogen gas into the sealed chamber.

Electrochemical Characterization: The electrochemical properties of AuNW and PEDOT:PSS assembled vertical devices were investigated by cyclic voltammetry (CV), galvanostatic charge/discharge (GCD), and electrochemical impedance spectroscopy (EIS) with a Biologic SP-200 potentiostat. The areal (C_A) was calculated from galvanostatic charge/discharge curves based on the following equations:

$$C_A = \frac{I_d}{A}\left(\frac{1}{\overline{dV/dt}}\right) \tag{5}$$

where I_d is the discharge current, A is the area (25 mm^2), d is the average thickness, $\overline{dV/dt}$ is an average derivative of the discharge voltage. The EIS measurements were performed using an ac voltage amplitude of 10 mV while sweeping the frequency from 100 kHz to 100 mHz. The ionic conductivity (σ_{ionic}) was calculated from

**ADVANCED
SCIENCE NEWS**

www.advancedsciencenews.com

**ADVANCED
MATERIALS
INTERFACES**

www.advmatinterfaces.de

$$\sigma_{ionic} = \frac{L}{Z'A} \qquad (6)$$

where Z' is the real part of impedance when the phase angle is near to zero, L and A are the distance between the two electrodes, and the area of the electrodes, respectively.

Supporting Information

Supporting Information is available from the Wiley Online Library or from the author.

Conflict of Interest

The authors declare no conflict of interest.

Data Availability Statement

The data that support the findings of this study are available in the supplementary material of this article.

[1] E. Miyako, C. Hosokawa, M. Kojima, M. Yudasaka, R. Funahashi, I. Oishi, Y. Hagihara, M. Shichiri, M. Takashima, K. Nishio, *Angew. Chem., Int. Ed.* **2011**, *50*, 12266.

[2] S. Han, N. U. H. Alvi, L. Granlöf, H. Granberg, M. Berggren, S. Fabiano, X. Crispin, *Adv. Sci.* **2019**, *6*, 1802128.

[3] G. J. Snyder, in *Energy Harvesting Technologies*, (Ed.: P. Shashank, D. J. Inman), Springer, Berlin **2009**, pp. 325–336.

[4] S. B. Riffat, S. A. Omer, X. Ma, *Renewable Energy* **2001**, *23*, 313.

[5] A. Al-zubaidi, X. Ji, J. Yu, *Sustainable Energy Fuels* **2017**, *1*, 1457.

[6] C. Gao, S. W. Lee, Y. Yang, *ACS Energy Lett.* **2017**, *2*, 2326.

[7] D. Zhao, H. Wang, Z. U. Khan, J. C. Chen, R. Gabrielsson, M. P. Jonsson, M. Berggren, X. Crispin, *Energy Environ. Sci.* **2016**, *9*, 1450.

[8] S. Horike, Q. Wei, K. Kirihara, M. Mukaida, T. Sasaki, Y. Koshiba, T. Fukushima, K. Ishida, *ACS Appl. Mater. Interfaces* **2020**, *12*, 43674.

[9] B. Kim, J. U. Hwang, E. Kim, *Energy Environ. Sci.* **2020**, *13*, 859.

[10] M. Bonetti, S. Nakamae, M. Roger, P. Guenoun, *J. Chem. Phys.* **2011**, *134*, 114513.

[11] D. Zhao, A. Würger, X. Crispin, *J. Energy Chem.* **2021**, *61*, 88.

[12] D. Zhao, A. Martinelli, A. Willfahrt, T. Fischer, D. Bernin, Z. U. Khan, M. Shahi, J. Brill, M. P. Jonsson, S. Fabiano, *Nat. Commun.* **2019**, *10*, 1093.

[13] M. Bonetti, S. Nakamae, B. T. Huang, T. J. Salez, C. Wiertel-Gasquet, M. Roger, *J. Chem. Phys.* **2015**, *142*, 244708.

[14] S. L. Kim, H. T. Lin, C. Yu, *Adv. Energy Mater.* **2016**, *6*, 1600546.

[15] X. Wu, B. Huang, Q. Wang, Y. Wang, *Chem. Eng. J.* **2019**, *373*, 493.

[16] S. Mardi, D. Zhao, N. Kim, I. Petsagkourakis, K. Tybrandt, A. Reale, X. Crispin, *Adv. Electron. Mater.* **2021**, *7*, 2100506.

[17] A. V. Volkov, K. Wijeratne, E. Mitraka, U. Ail, D. Zhao, K. Tybrandt, J. W. Andreasen, M. Berggren, X. Crispin, *Adv. Funct. Mater.* **2017**, *27*, 1700329.

[18] X. Crispin, F. L. E. Jakobsson, A. Crispin, P. C. M. Grim, P. Andersson, A. Volodin, C. Van Haesendonck, M. Van der Auweraer, W. R. Salaneck, M. Berggren, *Chem. Mater.* **2006**, *18*, 4354.

[19] S. Mardi, P. Cataldi, A. Athanassiou, *Appl. Phys. Lett.* **2022**, *120*, 033102.

[20] S. K. M. Jönsson, J. Birgerson, X. Crispin, G. Greczynski, W. Osikowicz, A. W. D. Van Der Gon, W. R. Salaneck, M. Fahlman, *Synth. Met.* **2003**, *139*, 1.

[21] G. Zotti, S. Zecchin, G. Schiavon, F. Louwet, L. Groenendaal, X. Crispin, W. Osikowicz, W. Salaneck, M. Fahlman, *Macromolecules* **2003**, *36*, 3337.

[22] D. Zhao, A. Sultana, J. Edberg, M. S. Chaharsoughi, M. Elmahmoudy, U. Ail, K. Tybrandt, X. Crispin, *J. Mater. Chem. C* **2022**, *10*, 2732.

[23] S. L. Kim, J.-H. Hsu, C. Yu, *Org. Electron.* **2018**, *54*, 231.

[24] L. Coustan, G. Shul, D. Belanger, *Electrochem. Commun.* **2017**, *77*, 89.

[25] U. Ail, M. J. Jafari, H. Wang, T. Ederth, M. Berggren, X. Crispin, *Adv. Funct. Mater.* **2016**, *26*, 6288.

[26] M. Xia, J. Nie, Z. Zhang, X. Lu, Z. L. Wang, *Nano Energy* **2018**, *47*, 43.

[27] N. Ohta, K. Nomura, I. Yagi, *J. Phys. Chem. C* **2012**, *116*, 14390.

[28] Y. Wang, E. Laborda, K. R. Ward, K. Tschulik, R. G. Compton, *Nanoscale* **2013**, *5*, 9699.

[29] V. Gueskine, M. Vagin, M. Berggren, X. Crispin, I. Zozoulenko, *Electrochem. Sci. Adv.* **2022**, https://chemistry-europe.onlinelibrary.wiley.com/doi/full/10.1002/elsa.202100191.

[30] T. Tevi, H. Yaghoubi, J. Wang, A. Takshi, *J. Power Sources* **2013**, *241*, 589.

[31] B. B. Sales, O. S. Burheim, S. Porada, V. Presser, C. J. N. Buisman, H. V. M. Hamelers, *Environ. Sci. Technol. Lett.* **2014**, *1*, 356.

[32] D. Zhao, A. Sultana, J. Edberg, M. S. Chaharsoughi, M. Elmahmoudy, U. Ail, K. Tybrandt, X. Crispin, *J. Mater. Chem. C* **2022**, *10*, 2732.

[33] K. Tybrandt, D. Khodagholy, B. Dielacher, F. Stauffer, A. F. Renz, G. Buzsáki, J. Vörös, *Adv. Mater.* **2018**, *30*, 1706520.